Influence of lightweight aggregates on the physical and mechanical residual properties of concrete subjected to high temperatures

Dashnor Hoxha, Georges Roufael, Anne-Lise Beaucour, Javad Eslami, Albert Noumowé

Influence of lightweight aggregates on the physical and mechanical residual properties of concrete subjected to high temperatures

Roufael Georges [(1)], Beaucour Anne-lise[(1)], Eslami Javad [(1)], Hoxha Dashnor[(2)], Noumowe Albert[(1)]

[(1)] CY Cergy Paris Université, Laboratoire de Mécanique et Matériaux du Génie Civil, 5 Mail Gay-Lussac, Neuville-sur-Oise, 95031 Cergy-Pontoise Cedex, France
[(2)] Université d'Orléans, Université de Tours, INSA Centre Val de Loire Laboratoire de Mécanique Gabriel Lamé Polytech Orléans, 8 rue Léonard de Vinci, 45072 Orléans, France

ABSTRACT

This research studies the high temperature behavior of lightweight aggregate concretes (LWAC) by providing a comprehensive study that regroups the physical, thermo-mechanical and mechanical properties of three different LWACs. Then these properties are compared to the properties of a normal-weight concrete (NWC) as well as to those of the mortar phase of these concretes, thus, enabling us to isolate and identify specific behaviors of the lightweight aggregates (LWA). Contrary to the normal weight aggregates, the LWAs showed a compatibility in thermal strain with the mortar phase, which led to fewer cracks in the interfacial transition zone (ITZ) and thus, it resulted in a divergence in behavior between LWACs and NWC, particularly for the residual permeability and tensile strength values. While LWACs generally exhibited lower decrease of failure strengths, and Young Modulus with temperature than NWCs, its Poisson's ratio was greatly decreased after 300°C.

Keywords: Lightweight Concrete, Expanded clay aggregate, Expanded shale aggregate, High Temperature, Thermal deformation, Residual mechanical properties,

1 INTRODUCTION

The first lightweight aggregates (LWA) used in construction by the Romans were natural aggregates derived from volcanic rocks, such as pumice. Today, lightweight aggregates can be manufactured using natural raw materials such as clay, shale and slate [1], [2]. Due to its low density, lightweight aggregate concrete (LWAC) is used in the construction of stadiums, long span bridges and even offshore platforms. On the other hand, and in order to meet the environmental challenges of the 21st century and the increasingly demanding thermal regulations like the French standards (RT 2012 & RT 2020), the structural lightweight concrete is being used to improve the energy efficiency in buildings. It can reduce heating energy needs up to 15%, by replacing traditional structural concrete [3]. This research work is a continuation of the work of [4] and [5] conducted at the Laboratory of Mechanics and Materials of Civil Engineering of CY Cergy Paris Université. It focuses on the behavior at high temperature of structural lightweight aggregate concretes, especially LWAC made of expanded clay and shale aggregates, in order to ensure a safer design of buildings regarding fire. The fire resistance

of concrete depends on the attained temperature [6], the duration of fire [7] and the heating rate as well as the material properties like the thermal conductivity and diffusivity, the porosity, the permeability, the failure strength and the elastic modulus. The effective design of concrete against fire need to consider both explosive spalling and loss of mechanical properties. The purpose of this research work is to provide further understanding of the influence of lightweight aggregates on the evolution of mechanical and physical concrete properties with respect to temperature. At material scale, the decay of mechanical and physical properties mostly depends on the physico-chemical reactions that take place during heating and on the thermal cracking induced between the paste and aggregate. Concrete is a heterogeneous material that have different physical and chemical reactions when exposed to high temperature. Around 80°C and up to 120°C the free water contained in the concrete evaporates and the decomposition of ettringite (60-80°C) takes place [8]. From 110°C to 170°C the decomposition of gypsum and the loss of water from part of the carboaluminate hydrates occur [8], [9]. While the dehydration of C-S-H gels contained in the hardened cement can last up to 350°C-450°C [8], [10], [11] other studies claim that C-S-H may suffer dehydration up to about 600ºC [12]. At 750°C, the transformation of C-S-H is complete into the nesosilicate form with a C2S stoichiometry close to larnite [10]. After 450°C the portlandite starts to decompose, followed by the decomposition of the calcite at around 700°C [8], [11], [13]. The behavior of the concrete is also greatly influenced by the aggregates as they occupy an important volume of the mixture (60 – 80%) [14], [15]. Artificial lightweight aggregates already heated during their manufacturing process, have good thermal stability. On the other hand, they are characterized by a higher porosity and a higher water absorption compared to ordinary aggregates, which will impact the thermo-physical and water transfer properties. The presence of lightweight aggregates can therefore affect the magnitude of the thermal gradient and the liquid and water vapor pressures within the concrete when it is subjected to high temperatures. In fact, the high porosity of lightweight aggregates leads generally to lower thermal conductivity [5], [16]–[18]. Depending on the type of LWA, the thermal conductivity of LWAC is 40–53% lower than that of NWC of the same composition [19]. Furthermore, the higher porosity of the lightweight aggregate leads to more porous concretes whose permeability increases more or less depending on the aggregate porous network and the presence or not of a thick outer shell. The porous structure within a lightweight aggregate can vary significantly from one type to another. It can range from a predominately closed porous structure (expanded shale) to mostly an open one (certain types of expanded clays and pumice) thus influencing the permeability and migration paths of fluids inside within the concrete.

Thermo-mechanical damage and in particular thermal cracking is influenced by the nature of the aggregates. During heating, cracking is initiated at the paste-aggregate interface due to the incompatibility of deformation between the paste and the aggregates on one hand, and the presence of

a porous Interfacial Transition Zone (ITZ) of lower resistance than the paste on the other hand [20]. The aggregates expand when heated, while the cement paste shrinks as a result of the dehydration of the hydrates from 120°C onwards. Due to their high porosity and thermal stability, lightweight aggregates have a lower expansion than ordinary aggregates. An increase of voids in the specimens depending on apparent porosity results in a significant decrease in thermal expansion due to decrease of internal thermal stress [21]. Another important role of the aggregate is its influence on the ITZ between the cement paste and the aggregate which can lead to an important change in physical and mechanical properties such as gas permeability and tensile strength. A porous ITZ can compromise the internal structure of the concrete creating a network of pores across the three-dimensional microstructure which may become an issue for the long-term durability of the material [22]. In this regard, studies have shown that using lightweight aggregate can enhance the ITZ due to a nonexistent wall effect between the mortar phase and the aggregate and the penetration of hydrated cement in the porous shell of the LWA creating interlocking sites [23], [24]. Furthermore, using LWA for the internal curing of concrete can reduce the volume fraction of the percolated ITZ paste [25], [26]. As for high temperature behavior, research already carried out on this subject showed that LWAC maintained slightly better mechanical properties compared to normal weight concrete (NWC) after an ISO fire [27], losing around 50% and 91% of its initial compressive and tensile strength respectively [28]. Sancak, Andic-Cakır and Karakoç [29]–[31] worked on pumice based lightweight aggregates. Sancak [29], showed that pumice based LWAC had up to 28% of relative compressive left at 800°C, double than that of NWC (16%). Furthermore, Andic-Cakır [30], by investigating the influence of high temperature on the mechanical properties of self-consolidating concretes found that cracks follow a weak and porous zone inside pumice aggregate instead of ITZ, while Karakoç [31] highlighted the impact of the cooling regime on the residual mechanical strength of LWAC. Moreover, Felicetti [32] attributed the difference in the tensile strength behavior between LWAC and NWC to the reduction of the kinematic incompatibility between the coarse aggregate and the cement paste due the expulsion of water from the LWA and the smaller stiffness of these aggregates. Yoon [33] confirmed the good resistance of LWAC at high temperature with the LWAC having lower thermal strain than NWC. As for the standards, the Eurocode 4 offers compressive strength, tensile strength and elastic modulus curves of LWAC as a function of temperature.

While most of the existing studies on the high temperature behavior of the LWAC have focused on a limited type of aggregate and/or a limited set of mechanical and thermal properties, few studies provide an explanation of the difference of behavior between NWC and LWAC at high temperatures, taking into account different density and nature of LWA. This work, tries to fill this gap by offering a comprehensive study that compares the properties of three different types of LWAC with a normal weight concrete (NWC) and the mortar matrix of these concretes, which enables us to isolate and

identify exclusive behavior of aggregates. It encompasses a large number of thermal, physical and mechanical properties that are essential to the analysis of high temperature behavior and/or are relevant to the assessment of concrete durability in a post fire situation. Furthermore, it provides a phenomenological approach by coupling the results with a microscopic analysis of the ITZ and the microstructure enabling us to study the influence of the aggregates on the cracking in the concretes.

2 MIXTURE PROPORTIONING AND EXPERIMENTAL APPROACH

2.1 Aggregates

Three coarse lightweight aggregates were tested: two expanded clay aggregates and one expanded shale aggregate. The lightweight aggregates studied have different oven-dried particle densities, 824 kg / m^3 for (AR-550), 1346 kg / m^3 for (AM-650) and 1320 kg / m^3 for (SE 4/8) determined according to EN 1097-6 (Table 1). Table 1 also presents the Saturated Surface Dry particle density and the apparent particle density. According to EN 1097-6, the apparent particle density is the ratio between the mass of grains dried and the volume that they occupy in water, including closed pores but excluding those accessible to water. Their water absorption after 48h ranges between 8.5% for S 4/8 and 28% for AR 550. As for the open porosity AM 650 have the highest percentage of open pores with 40.2% followed by AR 550 with 34.5% and finally S 4/8 with 18.5%. AR 550 has the highest closed pore percentage with a total porosity of 69% followed by 50.1% and 49.2% for S 4/8 and AM 650 respectively. The total porosity is calculated by considering the solid density of the aggregates equals to 2.65. The expanded clay aggregate (AR4/10-550) and the black limestone aggregate are of a 4/10 mm granular class whereas the expanded clay (AM4/8-650) and the expanded shale aggregates are of 4/8 mm class. The two expanded clay aggregates have different morphologies (Figure 1- a, b). While AR has a spherical shape with a defined external shell (180 – 323 µm) , AM on the other hand have a random geometry with a less apparent shell (150 – 220 µm). The expended shale on the other hand (Figure 1- c) have a well-defined and the thickest external shell on average (280 – 500 µm). The mortar phase consists of CEM I 52.5N cement and a silico-calcareous sand of 0/4 mm granular class. The cement has a density of 3140 Kg / m^3 and contains 97% clinker and 3% minority constituents.

Figure 1: Cross-section of the three lightweight aggregates

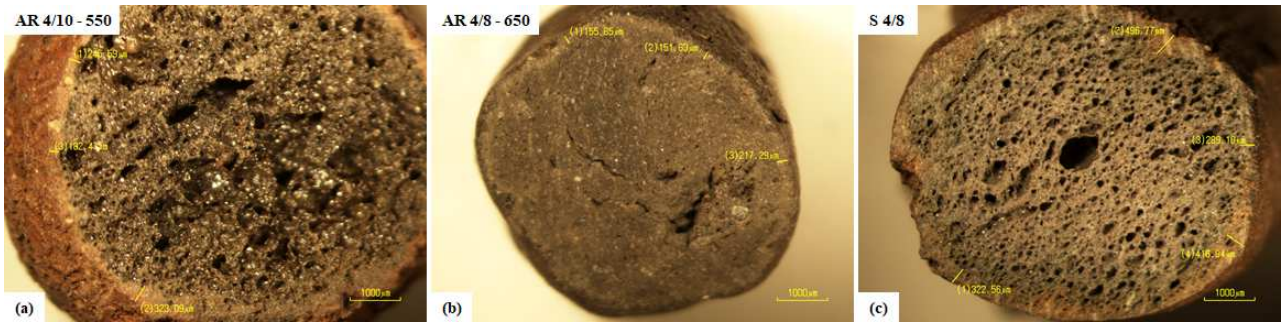

Table 1: Aggregate properties

Aggregates	Density [kg/m^3]			Porosity* [%]		Absorption after 48 h [%]	Granular class	Nature
	ρ_{Lrd} [a]	ρ_{Lssd} [b]	ρ_{La} [c]	P_o	P_T			
Sand SC	2570	-	-	2.6	-	1	0/4	Silico-calcareous
AR 4/10-550	824	1169	1258	34.5*	69	28	4/10	Expanded clay
AM 4/8-650	1346	1748	2250	40.2*	49.2	24.6	4/8	Expanded clay
S 4/8	1320	1500	1620	18.5*	50.1	8.5	4/8	Expanded shale
Black limestone	2710	-	-	1.4	-	0.51	4/10	Limestone

[a]Oven dry particle density
[b]Saturated surface dry particle density
[c]Apparent particle density
P_o : Open porosity
P_T : Total porosity
*Calculated after 1 month of immersion

The chemical composition of lightweight aggregates is provided by the producers. It was determined using X-ray fluorescence analysis (XRF). All aggregates consist of a large quantity of silica, from 60 to 63% with an important part consisting of alumina and Iron Oxide (Table 2).

Table 2: Chemical compositon (%) of the lightweight aggregates

Aggregates	SiO_2	Al_2O_3	Fe_2O_3	CaO	MgO	K_2O	Na_2O	SO_3	S	Mn_2O_3	TiO_2	P_2O_5
Expanded Shale	63.00	21.00	8.50	1.50		3.60	1.54	0.01	0.02	-	-	-
Expanded Clay	59.50	17.00	14.30	2.00	1.50	3.00	0.50	-	1.00	0.20	0.90	0.10

The mineralogy of expanded shale and clay aggregates are determined by the XRD analysis (Cu Ka radiation). The data from the analysis are reported from the work of Nguyen [5], [34]. The main mineral phases of expanded shale are quartz, iron oxide (magnetite) and potassium feldspar and albite. Clay aggregates mainly contain quartz, potassium feldspar, albite and iron oxide (magnetite and maghemite) and chabazite.

2.2 Mix design, specimens preparation and thermal cycles

Five mixtures were prepared, including two concretes with expanded clay coarse aggregate (LWCC1 made with AR 4/10 & LWCC2 made with AM 4/8), one with expanded shale coarse aggregate (LWSC made with S4/8)), a reference concrete with black limestone coarse aggregate (NWC made

with black limestone) and a mortar. This study considered concrete as a material that consists of two distinct phases, mortar and coarse aggregates. The mixtures were designed to maintain a constant volume of paste and aggregate for each type of aggregate and to ensure that the strength of the lightweight concretes was compatible with structural purpose, based on the results of [35]. The four concrete mixtures (Table 3) have the same water to cement ratio (W / C = 0.45) and the same volume fraction of coarse aggregate (37%) of the total volume concrete while the mortar has the same mix-design as the mortar matrix of the four concretes. It is thus possible to identify and isolate the exclusive behaviors of the lightweight coarse aggregates. The D_{max} of AR 550 is 10 mm and that of AM 650 and S 4/8 is 8 mm. This could affect the compactness of the granular skeleton. However, the slump values of the lightweight concretes are very close and show that the same workability (consistency) is obtained for each of the lightweight concretes. Thus we can make the hypothesis that the difference in D_{max} has little influence on the properties of the concrete.

Table 3: Mixture proportions of concrete per m3 (unit kg) and concrete properties

Concrete	Cement 52.5	Effective water	Coarse Aggregate ssd	Sand	Slump [mm]	Oven dry density [kg/m^3]	fc 90 [MPa]	λ [W/m.K]
LWCC1	426	192	369	777	70	1650 ± 14.9	31.6 ± 1.1	1.05
LWCC2	426	192	585	777	65	1850 ± 11.1	49 ± 3.1	1.07
LWSC	426	192	547	777	70	1800 ± 16.9	41 ± 2.6	1.05
NWC	426	192	1002	777	110	2260 ± 3.5	57.5 ± 8.4	1.90
Mortar	676	304	-	1233	-	2090 ± 5.9	58.8 ± 0.8	1.70

Due to the high absorption nature of the LWA, and in order to control the water-cement-ratio during mixing, aggregates were immersed in water during 48 hours before mixing and then drained for about 30 minutes until their surface moisture content became constant. Mixing water was then reduced by the quantity of water brought by the LWA surface moisture. The specimens were stored in wet rags and plastic bags for 90 days. The concretes tested have compressive strengths at 90 days ranging between 32 MPa for LWCC1, 41 MPa for LWSC, 49 MPa for LWCC2 and 58 MPa for NWC, with oven dry densities of 1650, 1800, 1850 and 2260 Kg / m^3 respectively. The various mechanical and physical tests were carried out after heating and cooling. The heating at 1 °C/min is followed by an isothermal stage of 2 hours at target temperatures of 150 °C, 300 °C, 450 °C, and 600 °C, in order to ensure a uniform temperature around the circumference of the test specimen and axially along the reference length [36]. The control thermocouples were placed on the surface of the specimens. As for cooling rate, the specimens are cooled at a rate of 1°C/min until around 150°C where this cooling rate cannot be imposed and the specimens are cooled at room temperature (Figure 2). Low heating and cooling rates are applied to limit the thermal gradient and to avoid any structural phenomenon, the objective being to provide temperature evolution laws of material properties.

Figure 2: The electrical furnace CMT (700°C) and the heating/cooling cycles at different temperature levels

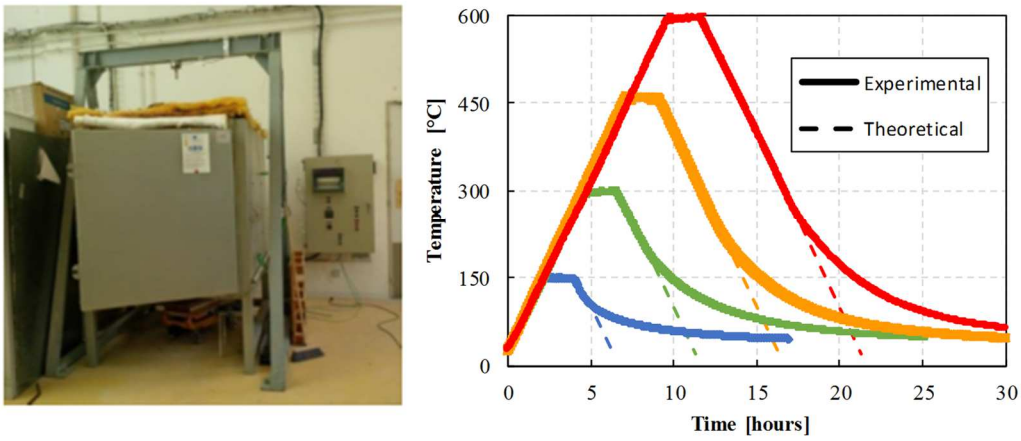

The furnace has a heating capacity of 750°C with a depth of 1.20 m, a length of 1.12 m and a height of 1.00 m. Both side walls are equipped with heating resistors. The back of the furnace is equipped with a fan to improve temperature homogenization. This furnace is equipped with a Eurothern 2404 thermal controller/programmer and a West 6700 control controller (Figure 2).

2.3 Tests after heating and cooling

The loss of mass was determined on an average of six 110Φ220 mm cylinders according to the following equation:

$$Loss\ of\ mass\ (\%) = \frac{(M_1 - M_2) \times 100}{M_1} \quad (1)$$

where M1 is the mass before heating and M2 the mass after heating.

The measurements of the density and the water accessible porosity under vacuum were carried out according to standard NF P 18-459. The test was performed on four samples for each type of concrete. For characterizations at room temperature, the samples were dried in the oven at 80 ° C to constant mass. Samples exposed to high temperature are tested immediately after the heating / cooling cycles.

The gas (nitrogen) permeability of the concretes was measured on 150Φ50 mm specimens using a Cembureau device [37]. For each target temperature level, 2 specimens were tested. The lateral surfaces of the specimens were coated with self-adhesive aluminum to ensure that the gas flow only passes through the bases of the specimen (sawn surfaces). Once the sample is in place, the inner tube is filled with gas up to a pressure of 8 bar. The lateral pressure is higher than the injection pressure to ensure the lateral support and sealing of the specimen. The specimen is ready to measure the apparent permeability after a stabilization time. The operating principle of the permeameter is based on the application of a constant pressure at the specimen inlet and the measurement of the gas (nitrogen) flow

rate at the inlet and outlet, after pressure stabilization, when the steady state is reached. The flow rates upstream and downstream of the sample were measured using a volumetric flowmeter. Figure 3 shows the complete gas permeability measurement system. The measurements were made at 20°C and a relative humidity of 75%.

Figure 3: Gas permeability measurement system

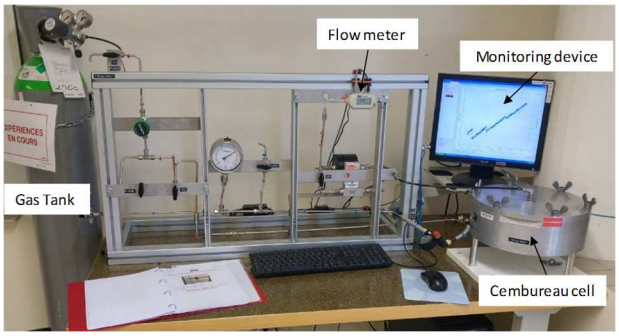

The apparent permeability Ka is determined according to the following formula:

$$K_a = \frac{2 \times \mu \times Q \times l \times P_{atm}}{A(P_1^2 - P_{atm}^2)} \quad (2)$$

with μ the dynamic viscosity of the nitrous oxide N_2 [Pa.s]; Q the volume flow rate of the gas at the outlet [m^3/s]; P_{atm} the atmospheric pressure [Pa]; l the thickness of the test body in [m]; A the sample cross-section in [m^2]; $P1$ the absolute gas pressure at the inlet in [Pa]. The intrinsic permeability K_{int} is deduced from the apparent permeabilities with the correction proposed by Klinkenberg [38]. The intrinsic permeability K_{int}, depending only on the viscous flow, acts on the entire volume contained in the capillary, or on the entire straight section considered, while the apparent permeability Ka also depends on the sliding flow (Figure 4). In this study, the determination of intrinsic permeability with Klinkenberg correction is obtained graphically by plotting the linear regression of the experimental points of apparent permeability Ka as a function of the inverse of the mean pressure $1/P_{moy}$.

Figure 4: Example of a permeability measurement

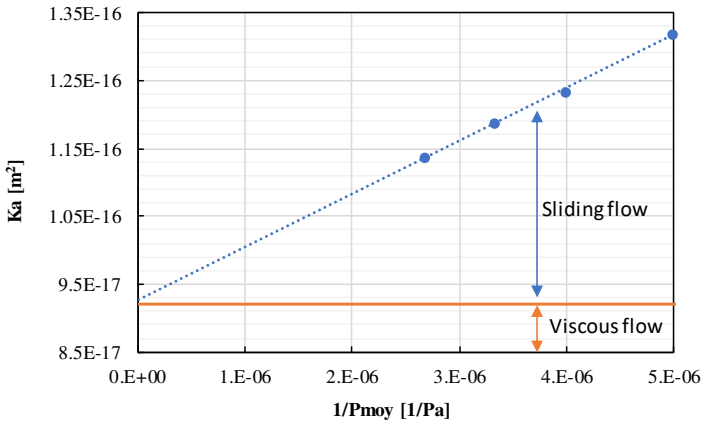

The velocity of P waves is measured on cylindrical samples 110Φ220 mm, using a Pundit. (Figure 5). The dynamic Young's modulus is then calculated using the following equations:

$$V_p = \frac{L}{t} \tag{3}$$

$$E_d = \frac{V_p^2 \, \rho(1+\vartheta)(1-2\vartheta)}{(1-\vartheta)} \tag{4}$$

where L is the length of material crossed (m); t the propagation time of the waves (s); ϑ the Poisson's ratio at the corresponding temperature measured by the strain gauges during a uniaxial compression test; ρ the density of the material at the corresponding temperature (Kg / m^3); V_p wave propagation velocity (m / s) and E_{dyn} dynamic Young's modulus.

Figure 5: Ultrasounic velocity measurement device

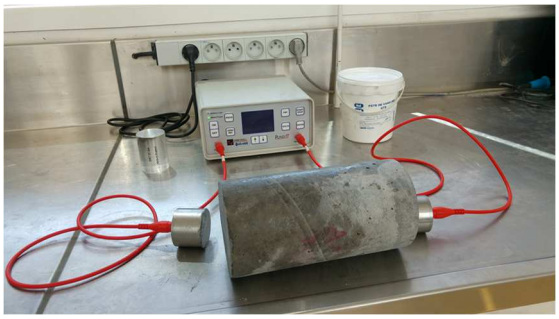

The uniaxial compression and splitting tensile tests are carried out on 110ϕ220 mm concrete cylinders using a hydraulic press according to NF EN 12390-3 and NF EN12390-6 standards respectively. At least three specimens where used to determine the mechanical properties for each concrete and target temperature. Two to three specimens were equipped with strain gauges to determine the static elastic modulus in accordance with EN 12390-13 during compression test. Four gauges were used on the cylinder, two attached axially and two attached transversally (Figure 6).

Figure 6: Prepared specimens with strain gauges

2.4 Dilatometry and thermal expansion test

The measurements of the deformation and the thermal expansion were carried out using a dilatometer DIL 402-PC (Figure 7), on cylindrical samples of 10 mm in diameter and 50 mm in length core drilled of 150Φ300 mm and 110Φ220 mm specimens. All samples were dried in the oven at 80°C prior to testing to ensure that any moisture that might affect the test was removed. Sample was pressed against sample holder by the pushrod (25 cN) with a thermocouple placed in direct proximity for temperature measurement. Pushrod was linked with a displacement sensor that measures thermal expansion during heating. To substract the expansion contribution of the sample holder and pushrod, a corretion measurement was carried out in the same conditions using a standard sample prior to measurement. The test was carried out for each type of concrete on three different samples in order to check the repeatability of the test. After measuring the initial length and calibrating the device, the samples were heated at a rate of 4°C / min from 20°C to 1050°C and then naturally cooled to room temperature.

Figure 7: Dil 402-PC device and an example of a sample used

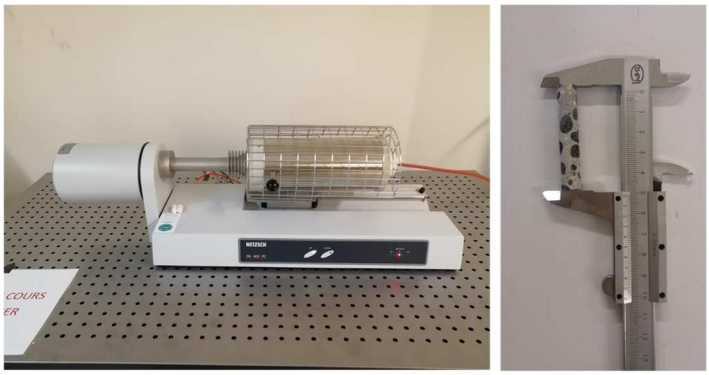

(a) (b)

2.5 Microstructural investigation

Observations using a scanning electron microscope are carried out on a ZEISS GeminiSEM 30 device, at a variable electron beam intensity depending on the type of observation and an acceleration voltage ranging between 2 kV and 15 kV. Two types of SEM observations were used in this study:

Observations on bulk specimen using secondary electron signal (SE), and observations on epoxy impregnated specimens using backscatterd-electron signal (BSE). The latter specimens and after an exposure to elevated temperatures were cut and dried at 45°C and 50% relative humidity for 48 h. Following the drying period, the specimens were impregnated with epoxy resin. The samples are then placed in small cylindrical plastic molds (diameter 4 cm and height 3 cm), then filled with epoxy resin. They are placed under vacuum in order to evacuate the air in the resin and then air-dried for 48 hours. Once the resin is dry, the samples are unmolded. All samples are polished in several steps until the resin layer has been well removed and the following. Prior to the SEM observations, the samples are metallized to make them conductive, using a Polaron SC502 metallizer. The SEM observations were also coupled with Energy Dispersive X-Ray spectroscopy analysis (EDS).

Other microscopic observations were conducted using a stereo microscope on the slices of cylinders used in the permeability tests.

3 RESULTS AND DISCUSSION

3.1 Thermal deformation and coefficient of thermal expansion (CTE)

The values in Figure 8 represent the average over three LWCC1 samples with its corresponding error bars. There was no significant variation from one test to another. Despite the small difference between the diameter of the sample and the maximum size of the aggregate, it can be considered that the measured result is representative of the material behavior due to the repetitiveness of the results for the three specimens. From 20°C to 530°C, the deformation increases almost linearly with the temperature for all concretes up to a value of 0.4% for lightweight concretes and silico-calcareous mortar, and 0.5% for NWC (Figure 9a). On the other hand, the coefficient of thermal expansion is more or less stable up to this temperature. It varies between 5 E-06 and 1 E-05 1/K for LWCC2, LWCC1, LWSC and the mortar, and between 1 E-05 and 1.5 E-05 for NWC (Figure 9b). At 570°C, there is a significant increase in deformation, due to the change of α phase of the quartz to its β phase [39] which results in a peak of the thermal expansion coefficient for all concretes and it reaches 1.7 E-04 1/K for mortar, followed by 1.2E-04, 1.0E-04, 9.1E-05 & 8.2E-05 1/K for LWCC1, LWSC, LWCC2 & NWC, respectively (Figure 9b). Note that the majority of the quartz comes from silico-calcareous sand and the rest comes from LWA (Table 2). After 600°C, the deformation stabilizes at 0.5% and then begins to decrease for lightweight concretes and mortar, while it increases rapidly for NWC after 700°C to reach 2% at 1000°C. At 700°C, the decarbonation of limestone aggregate takes place, usually this reaction results in an overall shrinkage of the material. But this shrinkage of the limestone aggregates generates high tension in the specimen creating cracks which translate to an irreversible deformation in the cooling phase. On the other hand, the shrinkage effect is noticed on the LWAC and the mortar by having a negative deformation at the end of the cooling phase. In general, a greater

expansion of limestone concrete compared to lightweight concrete is observed (even before 700°C). This can be attributed to a higher thermal expansion of the limestone aggregates compared to that of the mortar. Niry Razafinjato [15], [40] studied the high temperature behavior of black limestone aggregates. His results of the CTE and thermal deformation are represented in Figure 10. Between 20°C and 150°C the CTE of the limestone is lower than that of the mortar. After 150°C and up until 530°C the trends are reversed. While the CTE of the mortar stabilizes at around 5E-06 1/K, the CTE of the limestone continue to increase reaching 2.3E-05 1/K at 500°C (Figure 10b). This increase in CTE translates into a higher thermal deformation of the limestone compared to the mortar (Figure 10a). The lower thermal expansion of the mortar compared to that of the reference concrete can be explained by the higher porosity of the mortar and by the greater volume fraction of paste which tends to shrinkage after 120°C [20]. A higher amount of voids in the specimens depending on apparent porosity can result in a significant decrease in thermal expansion due to decrease of internal thermal stress [21]. The lightweight concretes undergo an expansion similar to that of the mortar suggesting a compatibility of thermal deformation between the silico-calcareous mortar and lightweight aggregates.

Figure 8: Average thermal deformation (dL/L_0 [%]-a) and average CTE (Alpha [1/K]-b) as a function of temperature for the LWCC1 (with error bars)

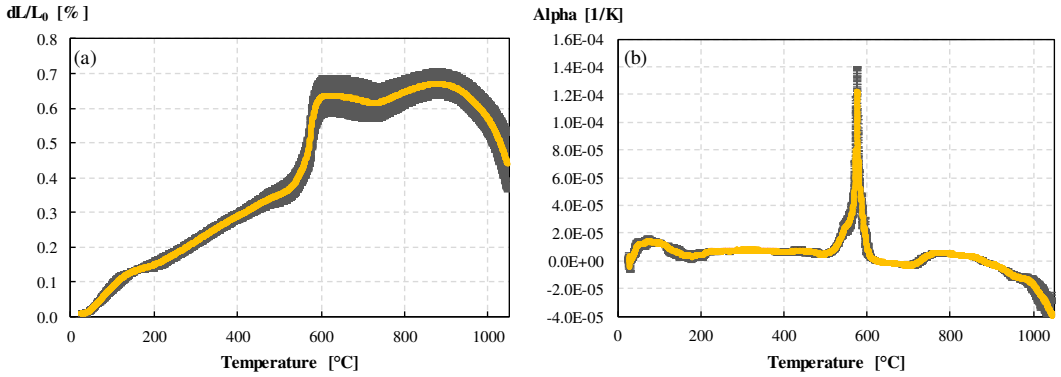

Figure 9: Average thermal deformation (dL/L_0 [%]-a) and average CTE (Alpha [1/K]-b) as a function of temperature for all concretes

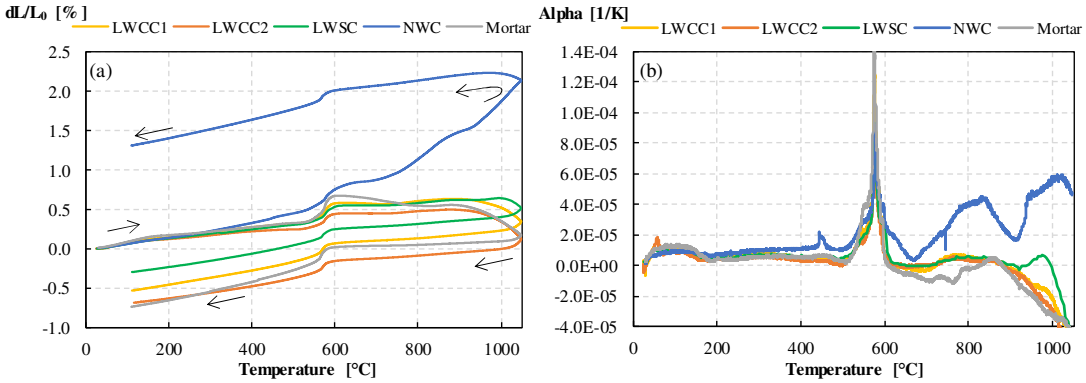

Figure 10: Average thermal deformation (dL/L_0 [%]-a) and average CTE (Alpha [1/K]-b) as a function of temperature for NWC, Mortar and black limestone aggregates [15], [40]

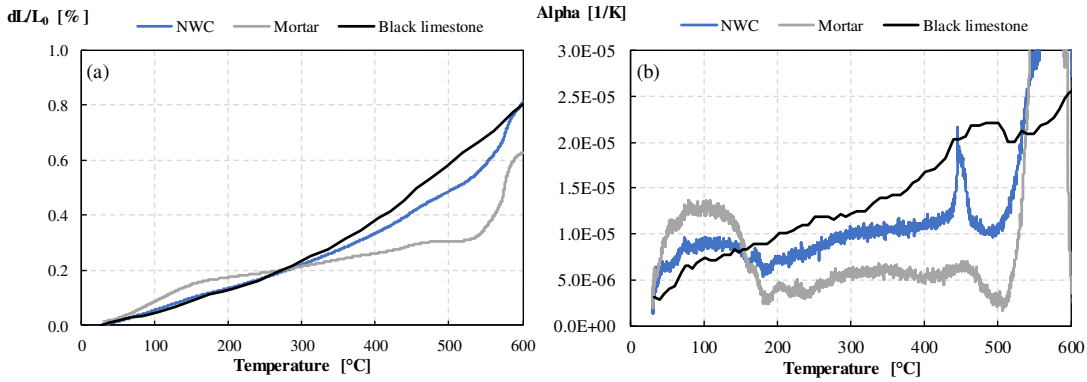

3.2 Study of residual physical properties and thermal cracking

Figure 11: Evolution of mass loss [%] as a function of temperature

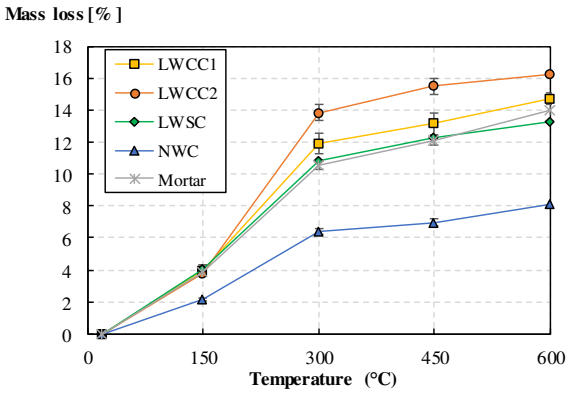

Mass loss curves show the same trend for all concretes (Figure 11). A significant loss of mass up to 300°C followed by a slight increase up to 600°C. Up to 300°C, this loss of mass is linked to the departure of free water and the dehydration of CSH and ettringite [8], [13]. After 300°C, the mass loss is relatively less important and is due mainly to the decomposition of the portlandite [41]. As the lightweight aggregates were saturated for 48 hours before the concrete was made, the total amount of water is higher and therefore the mass loss in the lightweight concretes is greater, 13.5%, 14.5% and 16% at 600°C for LWSC, LWCC1 and LWCC2, respectively. The mortar suffers a loss of 14%, higher than the 8% loss of the normal weight concrete. The difference between the mortar and the normal weight concrete can explained by the greater volume fraction of cementitious paste in the mortar as the majority of the weight loss occurs in paste [11], [15], [42].

The evolution of porosity as a function of temperature is represented in Figure 12. There is no significant variation up to 150°C except for LWSC concrete. At 300°C, an increase of 2% to 6% is noted. Subsequently, the porosity continues to increase to reach at 600°C, 8% and 12.5% for NWC

and LWCC2 respectively and 11.5% for LWSC and the mortar. The increase in porosity in lightweight concrete is about 4% higher than that of the normal weight concrete. This could be related to the development of cracks within the lightweight aggregates (Figure 16), giving access to pores formerly closed. Note that the curve of LWCC1 is higher than that of LWCC2 even though the open porosity for the corresponding aggregate (AR-550) is lower than the porosity of its counterpart (AM) (Table1).

Figure 12: Evolution of porosity (Porosity [%] – a), Porosity increase (P-P_0 [%] – b) as a function of temperature (P0 : initial porosity, P: porosity at a given temperature level)

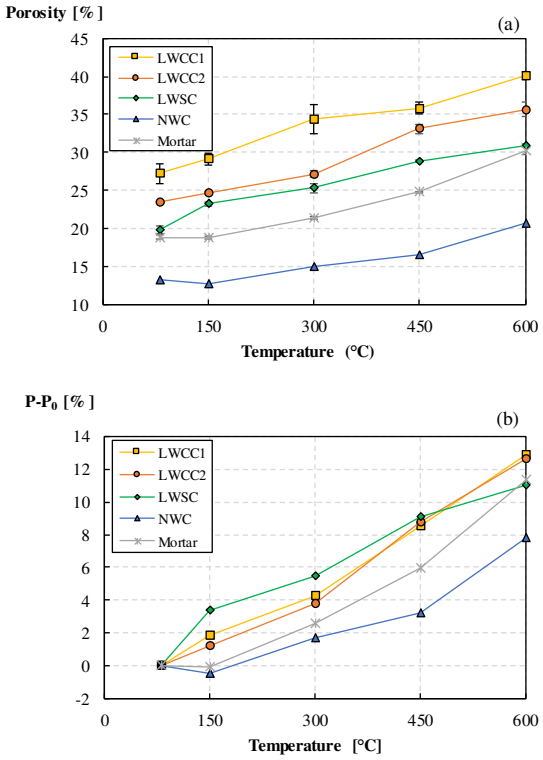

This result seemingly paradoxical can be explained by the fact that porosity of the aggregates is obtained through natural saturation whereas the porosity of the concrete is obtained through saturation under vacuum conditions. Thus, a greater part of the total porosity of AR-550 is accessible using the vacuum saturation approach. The order of the porosity values of the three lightweight concretes are thus consistent with the order of the values of the total porosity of the aggregates.

In regard to the density (ρ [Kg/m^3] - Figure 13), the concretes lose at 600°C, between 3.6% to 7% of their initial oven-dry density, LWCC2 and LWSC being the most affected followed respectively by the mortar, LWCC1 and then NWC. As the majority of the weight loss is associated to the mortar phase which is the main contributor to the LWAC weight, and the aggregates occupy the same volume fraction in all concrete mixtures, it is expected that the oven-dry density of the LWAC would be more affected than its NWC counterpart.

Figure 13: Evolution of dry density (ρ_{amb} [Kg/m^3] – a), relative dry density ($\rho_{T°}/\rho_{amb}$ [%] – b) as a function of temperature

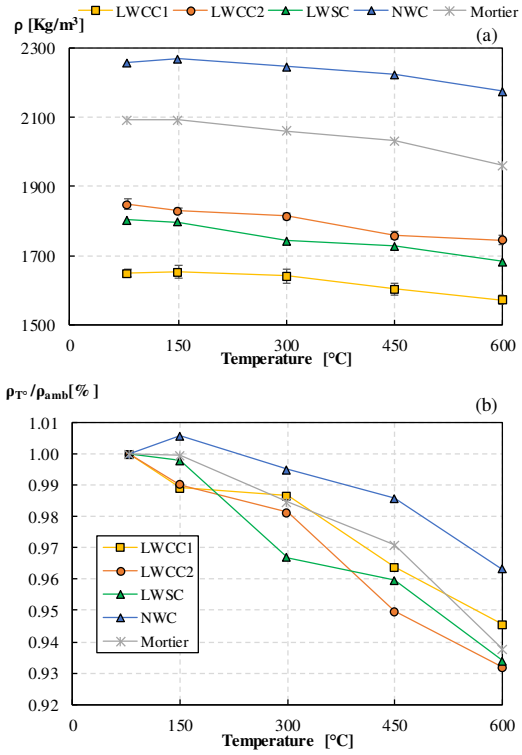

The results of the permeability measurements reported in Figure 14a, show that the LWAC are more permeable than NWC and Mortar at 150°C with values varying between 8.10^{-17} m² and 1.10^{-18} m². These results are coherent with the values reported by Real [43] for the LWAC and NWC with a water-cement ratio equal to 0.45. At 300°C, the permeability values of the normal weight concrete and the mortar are multiplied by 10 and join those of lightweight concretes which undergo a very slight increase. At 600°C, the permeability for the normal weight concrete and the mortar (10^{-12} m^2) is greater than for lightweight concretes (10^{-15} m^2 <Kint <10^{-14} m^2). In the same way, according to [44] the permeability of normal weight concretes increases to 10^{-13} m^2 at 600°C, which is higher than 10^{-14} m^2 measured for lightweight concrete. Despite a higher increase in porosity for LWCC1, LWCC2 and LWSC, there is not a same trend for permeability and therefore the new accessible pores are rather intragranular pores within the lightweight aggregates that do not participate in the transfer processes. Conversely, for NWC and mortar, the porosity is initiated at the paste-aggregate interface and grows in the cement paste, thus creating a connected porous network (Figure 15).

Figure 14: Evolution of permeability (Kint [m²] - a), P wave velocity ($V_{T°}/V_{20°}$ - b) as a function of temperature

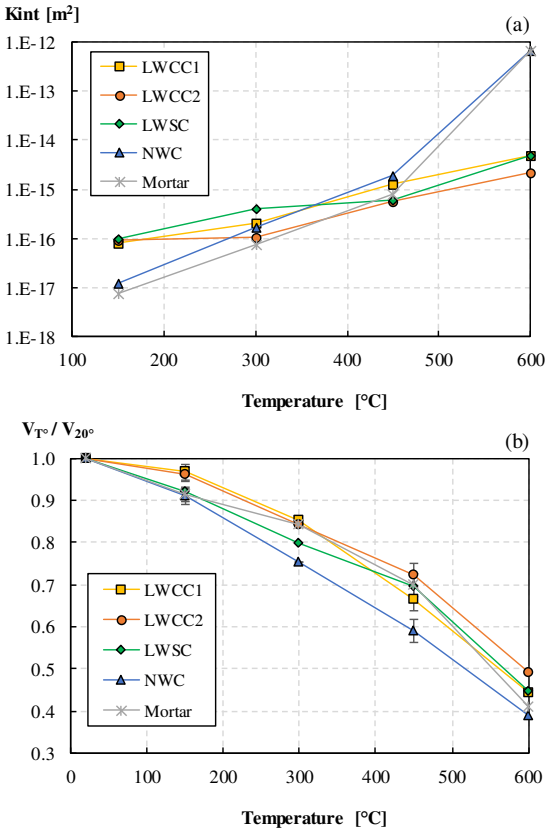

The relative evolution of ultrasonic wave velocities ($V_{T°}/V_{20°}$) is similar to that of the permeability, with earlier and more significant degradation of the normal weight concrete with temperature (Figure 14b). The mortar behaves like lightweight aggregate concrete up to 450°C. After this temperature, the mortar undergoes a significant drop in wave velocity coupled with an increase in porosity (Figure 12). At 600°C, the wave velocity of NWC decreases by 60% and only by 50% and 45% for the three lightweight aggregate concretes. Even though, the LWAC exhibits higher increase in porosity compared to NWC, the increase in its wave velocity is more moderate. This result confirms the result of the permeability and indicates a higher depreciation of ITZ [45] in the NWC.

Figure 15: Paste/aggregate interface of LWCC1 (a) and NWC (b) heated at 450°C

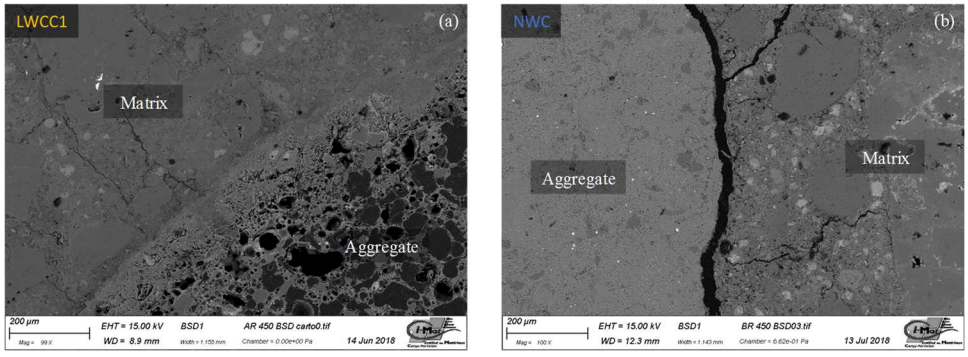

Figure 16: Cracks inside the lightweight aggregate at 450°C (LWCC1)

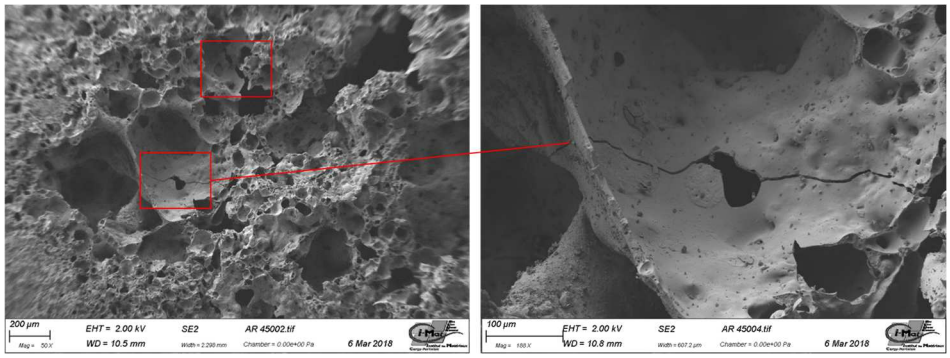

Figure 17: Cracks in concrete LWCC2 (a) and NWC (b) heated at 600°C

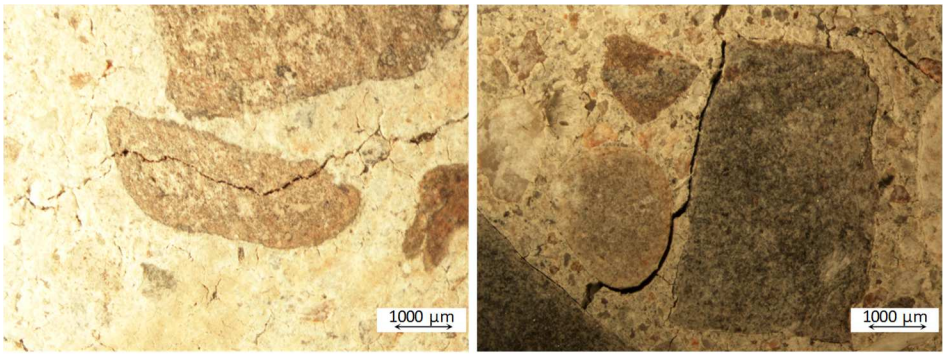

In order to understand the origin of the increase in permeability, the previous measurements were coupled with observations under both a stereo microscope and a scanning electron microscope. It has been found that the paste-aggregate interface is more damaged at 450°C for normal weight concrete than for the lightweight concretes (Figure 15). Also, at this temperature, cracks inside the LWA were observed (Figure 16). Similar observation was reported by Andiç-Cakir [30] who noted thermal cracks inside pumice aggregates after 300°C. In addition, observations with the naked eye and stereo-microscope of concretes heated up to 600°C (Figure 17), shows that the majority of cracks in lightweight concretes are transgranular while cracks in the normal weight concrete go through the interfacial area between the cementitious matrix and the aggregate. This can be explained by a more resistant paste-aggregate bond with porous lightweight aggregates than with limestone aggregates [4] and a better thermal deformation compatibility between the cementitious matrix and the aggregate (Figure 9). This better bond was confirmed using EDS analysis on the paste-aggregate interface of the LWA (Figure 18). The result shows a penetration of the paste inside the aggregate surface creating interlocking sites between the two entities.

Figure 18: Ca-Si Cartography using EDS analysis on the paste-aggregate interface of LWCC1

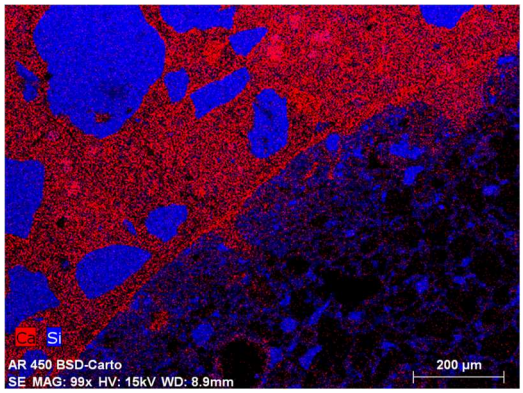

3.3 Residual mechanical properties

By substituting normal weight aggregates with lightweight aggregates, a drop in resistance is noticed since strength is mainly linked to the lightweight aggregate's failure strength [4]. At room temperature, the compressive strength of the concretes ranges between 58 MPa for NWC and 32 MPa for LWCC1 (Figure 19). Up to 300 °C, there is a slight loss of residual compressive strength for all concretes with a typical behavior of losing then gaining some strength at 150°C and 300°C respectively [10], [46], [47]. Beyond this, the compressive strength decreases rapidly for all the concretes but in a more moderate way for the lightweight concretes than for the reference concrete. At 450°C, the compressive strength of LWCC2 and LWSC become similar to NWC while the mortar shows a very good behavior up to this temperature by losing only around 10 % of its initial strength before quickly degrading at 600°C and losing 50% of its compressive strength. The lightweight aggregate concretes follow the same trend but with 20% less loss than the reference concrete. The difference in behavior between lightweight and limestone aggregates concretes is even more noticeable with the evolution of residual tensile strength (Figure 20).

Figure 19: Residual compressive strength ($f_{c,T°}$ [Mpa] – a), Relative residual compressive strength ($f_{c,T°}$/ $f_{c,T°amb}$ [-] – b) as a function of temperature

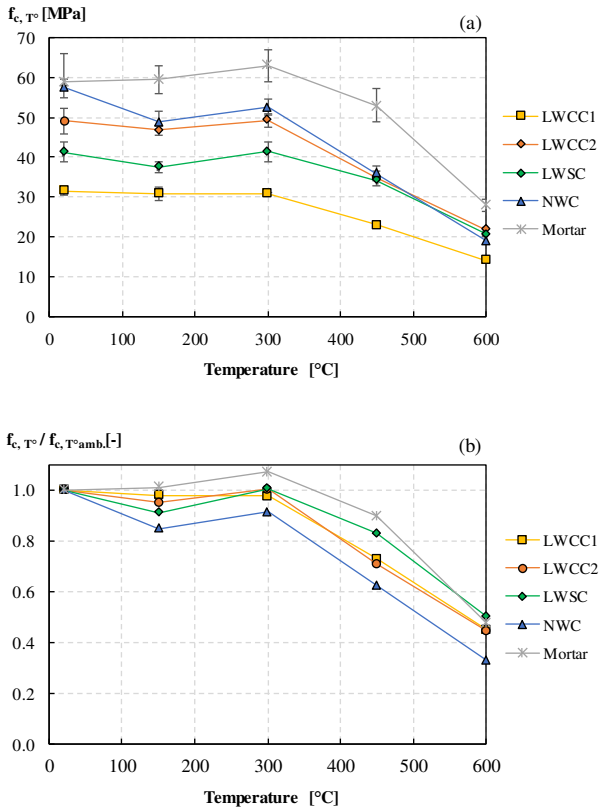

Unlike the normal weight concrete whose tensile strength decreases almost linearly with temperature, lightweight aggregate concrete and mortar show only, at 450°C, a slight loss of tensile strength of about 20 %, while NWC has lost more than 60 % of its initial strength. At this temperature, the absolute tensile strength of all lightweight concretes becomes higher than that of normal weight concrete. This can be explained by the good resistance of the paste-aggregate interface (Figure 15 & Figure 17) during the thermal loading related to a thinner and less porous Interfacial Transition Zone (ITZ) [23], [48]. Moreover the smaller thermal expansion of the lightweight aggregates compared to the calcareous aggregate limits the differential strain between the mortar and the aggregate and therefore the stress increase at the paste-agregate interface (Figure 9). Figure 21 shows that the crack path on the failure plane of the splitting test depends on the nature of aggregate and on the heating temperature. In concrete with limestone aggregate, the crack path is predominantly intergranular while in lightweight concretes transgranular cracks are mostly observed. With increasing temperature, the crack path becomes more and more intergranular (Figure 21), which means that the tensile strength is highly dependent on the interfacial zone's strength at higher temperatures. At these temperatures, the ITZ is weakened due to the dehydration of the cement paste and the decomposition of the portlandite coupled with an increase in thermal strain due to aggregate expansion.

Figure 20: Residual splitting tensile strength ($f_{t,T°}$ [Mpa] – a), relative residual splitting tensile strength ($f_{t,T°}$/ $f_{t,T°amb}$ [-] – b) as a function of temperature

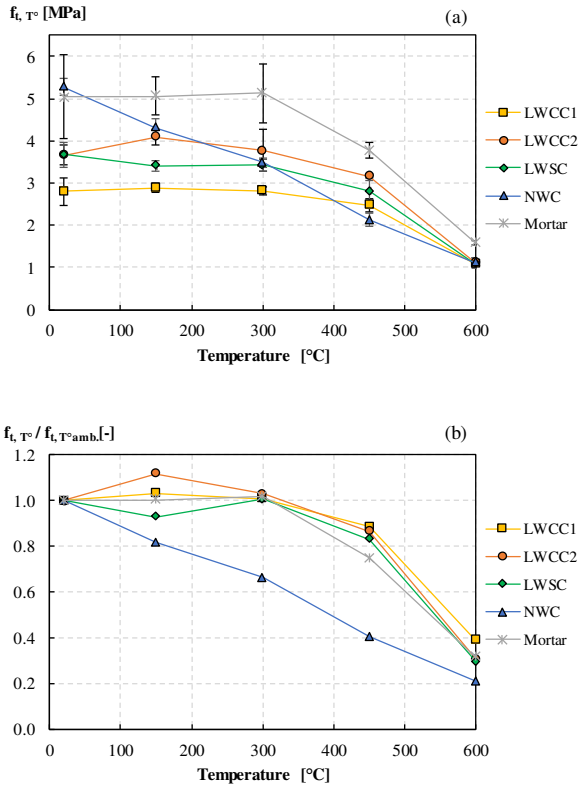

Figure 21: Evolution of the rupture plane after a splitting tensile test on 110ϕ220 specimens with respect to temperature

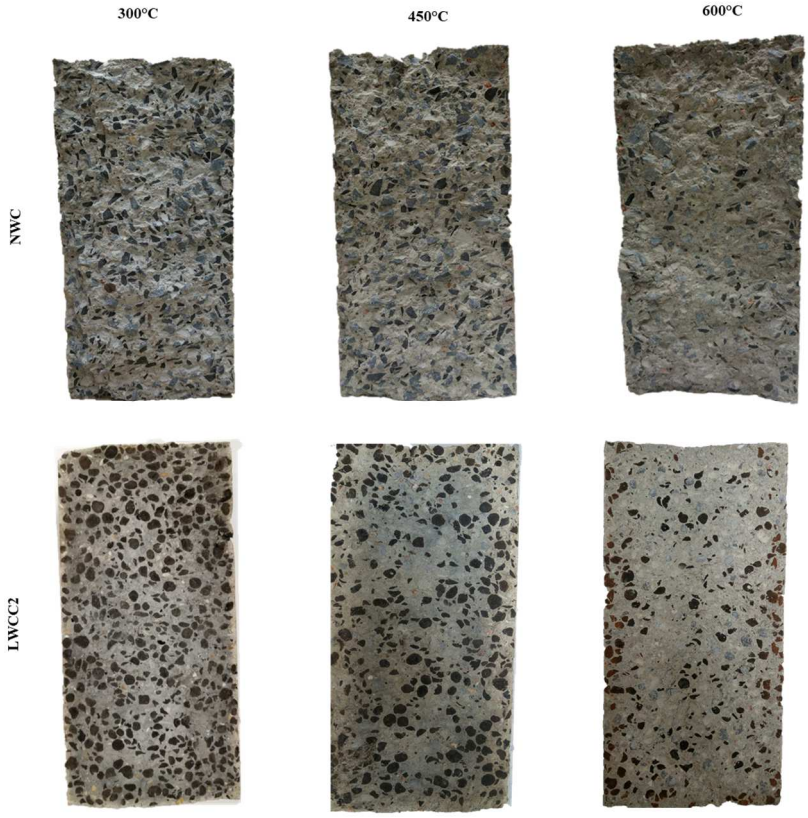

Figure 22: Residual static Young modulus ($E_{s,T°}$ [GPa] - a), relative residual static Young modulus ($E_{s,T°}$/ $E_{s,T°amb}$ [-] - b) as a function of temperature

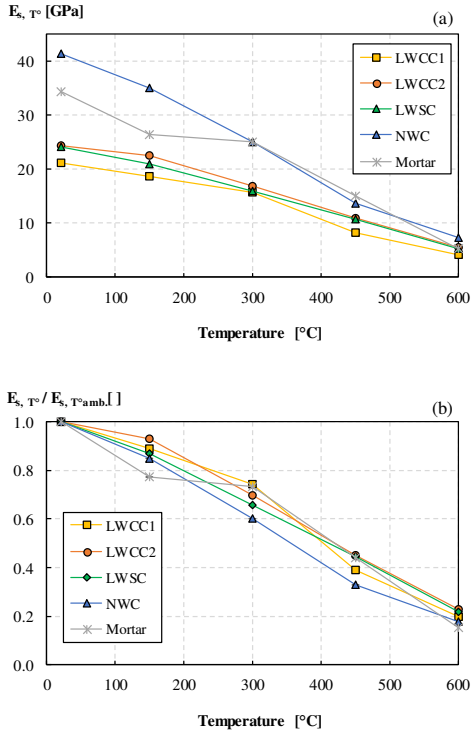

Figure 23: Residual Poisson's ratio (ν [-]) as a function of temperature.

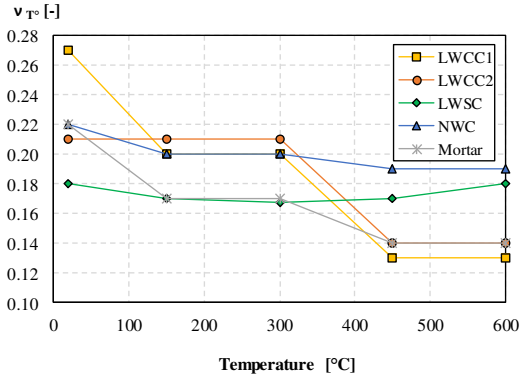

The static Young's modulus decreases more linearly with temperature than the tensile and compressive strengths (Figure 22). The static modulus loss is lower for lightweight aggregate concrete and mortar than for the normal weight concrete, especially between 150 and 450°C. Similar trends and losses in mechanical strength have been observed by Toriç [49]. On the other hand, Poisson's ratio undergoes a significant drop after 300 °C for lightweight clay aggregate concrete while that of the reference concrete and LWSC is not affected very much by the temperature (Figure 23). In order to better understand the evolution of the Poisson's ratio, the linear phase of the stress-strain curve was plotted at 300°C and 450°C for the NWC and the LWCC1 (Figure 24). While both concretes showed similar increase in axial deformation between 300°C and 450°C, the LWCC1 showed nearly no increase in lateral deformation. This result explains the drop in Poisson's ratio as there was no increase in the lateral deformation to compensate the increase of the axial deformation like in the case of NWC. The higher increase in the porosity of the mortar, of the LWCC1 and of the LWCC2 between 300°C and 450°C explains the decrease in its Poisson's ratios over this range of temperature.

Figure 24: Stress (σ [MPa]) vs strain (ε [µm/m]) for LWCC1 and NWC at 300°C and 450°C

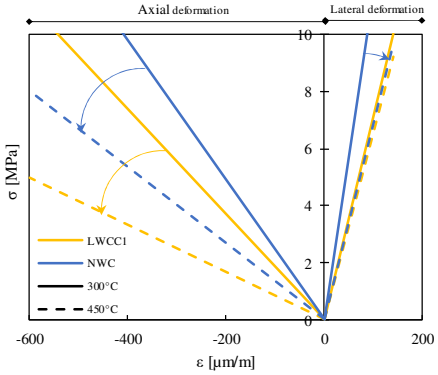

Figure 25: Dynamic Young modulus (Edyn [GPa]) vs static Young modulus (Estat [GPa])

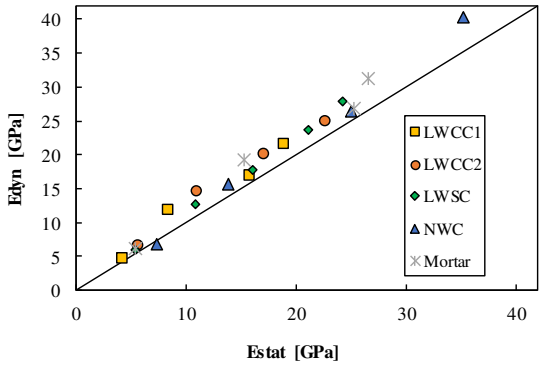

The comparison of the dynamic modulus (Edyn) with the static modulus (Estat) for the different target temperatures shows that the moduli are very close or identical at 600 °C (Figure 25). For the rest of the temperatures, the dynamic modulus was slightly overestimated when compared to the static modulus with a maximum difference recorded of 4 GPa for the NWC at ambient temperature. Overall, the wave velocity method accurately reflects the evolution of Young's modulus as a function of temperature.

4 CONCLUSIONS

The objective of this work is to study the behavior of LWAC when exposed to high temperature. This objective was achieved by measuring the evolution of properties with respect to temperature (Thermal, physical and mechanical) of three types of LWAC and comparing them to the properties of a reference concrete and a mortar. At a slow heating rate of 1°C/min, the hydric effects (the vapor and liquid pressure) and thermal gradients were reduced in the heated concrete and mortar specimens. Under these conditions, and based on the previous results, it is possible to conclude the following:

- The lightweight concretes studied showed a loss of failure strengths and Young's modulus with temperature more moderate than the reference calcareous aggregate concrete.
- Unlike the normal weight concrete whose tensile strength decreases almost linearly with temperature, lightweight aggregate concrete and mortar show only, at 450°C, a slight loss of tensile strength of about 20 %, while normal weight concrete has lost more than 60 % of its initial strength.
- Poisson's ratio undergoes a significant drop after 300°C for lightweight clay aggregate concrete while that of the normal weight concrete and expanded shale concrete is not affected very much by the temperature.
- The permeability of normal weight concrete increases faster with temperature than that of LWACs. At 600°C, the permeability of the normal weight concrete and the mortar became greater than for the three tested lightweight concretes.

- SEM and optical microscope observations have shown that the distribution and the cracking path after splitting test depend on the nature of the aggregates: intergranular for calcareous aggregates and transgranular for expanded shale and clay concretes. With increasing temperature, the crack path becomes more and more intergranular in lightweight concretes.

- From 300°C lightweight aggregates concrete showed a lower thermal expansion than the calcareous aggregate concrete after 300 °C.

- The expansion of the mortar constituting the matrix of concretes was similar to that of lightweight aggregate concrete, which shows a good compatibility of deformation between the mortar and lightweight aggregates.

- The better residual behavior of LWAC can be explained by a more resistant paste-aggregate bond with porous lightweight aggregates than with limestone aggregates and a better thermal deformation compatibility between the cementitious matrix and the aggregate

- Finally, despite lightweight aggregates of different densities and microstructure, lightweight aggregate concretes showed similar evolution of residual properties with temperature.

ACKNOWLEDGEMENTS

This work was supported by CY Cergy Paris Université and Université d'Orléans. The authors are grateful to ARGEX NV and GRANULEX to supply lightweight aggregates, to Annelise Cousture for SEM images and to Lilian Cristofol for help in the laboratory.

REFERENCES

[1] S. Chandra and L. Berntsson, "2 - Production of Lightweight Aggregates and Its Properties," in *Lightweight Aggregate Concrete*, S. Chandra and L. Berntsson, Eds. Norwich, NY: William Andrew Publishing, 2002, pp. 21–65.

[2] R. de'Gennaro *et al.*, "Structural concretes with waste-based lightweight aggregates: from landfill to engineered materials," *Environ. Sci. Technol.*, vol. 43, no. 18, pp. 7123–7129, 2009.

[3] S. Real, M. G. Gomes, A. Moret Rodrigues, and J. A. Bogas, "Contribution of structural lightweight aggregate concrete to the reduction of thermal bridging effect in buildings," *Constr. Build. Mater.*, vol. 121, pp. 460–470, Sep. 2016, doi: 10.1016/j.conbuildmat.2016.06.018.

[4] Y. Ke, S. Ortola, A. L. Beaucour, and H. Dumontet, "Micro-stress analysis and identification of lightweight aggregate's failure strength by micromechanical modeling," *Mech. Mater.*, vol. 68, pp. 176–192, Jan. 2014, doi: 10.1016/J.MECHMAT.2013.09.005.

[5] L. H. Nguyen, A.-L. Beaucour, S. Ortola, and A. Noumowé, "Influence of the volume fraction and the nature of fine lightweight aggregates on the thermal and mechanical properties of structural concrete," *Constr. Build. Mater.*, vol. 51, pp. 121–132, Jan. 2014, doi: 10.1016/J.CONBUILDMAT.2013.11.019.
[6] M. a. Riley, "Possible new method for the assessment of fire–damaged concrete," *Mag. Concr. Res.*, vol. 43, no. 155, pp. 87–92, Jun. 1991, doi: 10.1680/macr.1991.43.155.87.
[7] A. M. Neville, *Properties of concrete*, 5th ed. Harlow, England ; New York: Pearson, 2011.
[8] A. Noumowe, "Effet de hautes températures (20-600°C) sur le béton : cas particulier du béton a hautes performances," thesis, Lyon, INSA, 1995.
[9] L. Alarcon-Ruiz, G. Platret, E. Massieu, and A. Ehrlacher, "The use of thermal analysis in assessing the effect of temperature on a cement paste," *Cem. Concr. Res.*, vol. 35, no. 3, pp. 609–613, Mar. 2005, doi: 10.1016/j.cemconres.2004.06.015.
[10] G. A. Khoury, "Compressive strength of concrete at high temperatures: a reassessment," *Mag. Concr. Res.*, vol. 44, no. 161, pp. 291–309, Dec. 1992, doi: 10.1680/macr.1992.44.161.291.
[11] C. Alonso and L. Fernandez, "Dehydration and rehydration processes of cement paste exposed to high temperature environments," *J. Mater. Sci.*, vol. 39, no. 9, pp. 3015–3024, May 2004, doi: 10.1023/B:JMSC.0000025827.65956.18.
[12] N. Giraudo, S. Bergdolt, F. Laye, P. Krolla, J. Lahann, and P. Thissen, "Dehydration and dehydroxylation of C-S-H phases synthesized on silicon wafers," *Appl. Surf. Sci.*, vol. 433, pp. 589–595, Mar. 2018, doi: 10.1016/j.apsusc.2017.10.039.
[13] M. Castellote, C. Alonso, C. Andrade, X. Turrillas, and J. Campo, "Composition and microstructural changes of cement pastes upon heating, as studied by neutron diffraction," *Cem. Concr. Res.*, vol. 34, no. 9, pp. 1633–1644, Sep. 2004, doi: 10.1016/S0008-8846(03)00229-1.
[14] Z. Xing, A.-L. Beaucour, R. Hebert, A. Noumowe, and B. Ledesert, "Aggregate's influence on thermophysical concrete properties at elevated temperature," *Constr. Build. Mater.*, vol. 95, pp. 18–28, Oct. 2015, doi: 10.1016/J.CONBUILDMAT.2015.07.060.
[15] R. Niry Razafinjato, A.-L. Beaucour, R. L. Hebert, B. Ledesert, R. Bodet, and A. Noumowe, "High temperature behaviour of a wide petrographic range of siliceous and calcareous aggregates for concretes," *Constr. Build. Mater.*, vol. 123, pp. 261–273, Oct. 2016, doi: 10.1016/j.conbuildmat.2016.06.097.
[16] K. Lo-shu, S. Man-qing, S. Xing-sheng, and L. Yun-xiu, "Research on several physico-mechanical properties of lightweight aggregate concrete," *Int. J. Cem. Compos. Lightweight Concr.*, vol. 2, no. 4, pp. 185–191, Dec. 1980, doi: 10.1016/0262-5075(80)90036-6.
[17] S. Mindess, J. F. Young, and D. Darwin, *Concrete*, 2nd ed. Upper Saddle River, NJ: Prentice Hall, 2003.
[18] H. Uysal, R. Demirboğa, R. Şahin, and R. Gül, "The effects of different cement dosages, slumps, and pumice aggregate ratios on the thermal conductivity and density of concrete," *Cem. Concr. Res.*, vol. 34, no. 5, pp. 845–848, May 2004, doi: 10.1016/j.cemconres.2003.09.018.
[19] S. Real, J. A. Bogas, M. da G. Gomes, and B. Ferrer, "Thermal conductivity of structural lightweight aggregate concrete," *Mag. Concr. Res.*, vol. 68, no. 15, pp. 798–808, Aug. 2016, doi: 10.1680/jmacr.15.00424.
[20] F. al Nahhas, "Comportement thermo-mécanique des murs en maçonnerie de blocs creux en béton sous l'action d'un feu conventionnel," thesis, Université de Marne-la-Vallée, 2004.
[21] T. Uygunoğlu and İ. B. Topçu, "Thermal expansion of self-consolidating normal and lightweight aggregate concrete at elevated temperature," *Constr. Build. Mater.*, vol. 23, no. 9, pp. 3063–3069, Sep. 2009, doi: 10.1016/j.conbuildmat.2009.04.004.
[22] D. N. Winslow, M. D. Cohen, D. P. Bentz, K. A. Snyder, and E. J. Garboczi, "Percolation and pore structure in mortars and concrete," *Cem. Concr. Res.*, vol. 24, no. 1, pp. 25–37, Jan. 1994, doi: 10.1016/0008-8846(94)90079-5.
[23] M.-H. Zhang and O. E. Gjørv, "Microstructure of the interfacial zone between lightweight aggregate and cement paste," *Cem. Concr. Res.*, vol. 20, no. 4, pp. 610–618, Jul. 1990, doi: 10.1016/0008-8846(90)90103-5.
[24] T. Y. Lo and H. Z. Cui, "Effect of porous lightweight aggregate on strength of concrete," *Mater. Lett.*, vol. 58, no. 6, pp. 916–919, Feb. 2004, doi: 10.1016/j.matlet.2003.07.036.
[25] D. Cusson and T. Hoogeveen, "Internal curing of high-performance concrete with pre-soaked fine lightweight aggregate for prevention of autogenous shrinkage cracking," *Cem. Concr. Res.*, vol. 38, no. 6, pp. 757–765, 2008, doi: 10.1016/j.cemconres.2008.02.001.
[26] D. P. Bentz, "Influence of internal curing using lightweight aggregates on interfacial transition zone percolation and chloride ingress in mortars," *Cem. Concr. Compos.*, vol. 31, no. 5, pp. 285–289, May 2009, doi: 10.1016/j.cemconcomp.2009.03.001.

[27] F. K. Kong and R. H. Evans, “Properties of structural concrete,” in *Reinforced and Prestressed Concrete*, Boston, MA: Springer US, 1987, pp. 18–67.
[28] L. Bodnárová, R. Hela, M. Hubertová, and I. Nováková, “Behaviour of Lightweight Expanded Clay Aggregate Concrete Exposed to High Temperatures,” vol. 8, no. 12, pp. 1151–1154, 2014.
[29] E. Sancak, Y. Dursun Sari, and O. Simsek, “Effects of elevated temperature on compressive strength and weight loss of the light-weight concrete with silica fume and superplasticizer,” *Cem. Concr. Compos.*, vol. 30, no. 8, pp. 715–721, Sep. 2008, doi: 10.1016/j.cemconcomp.2008.01.004.
[30] Ö. Andiç-Çakır and S. Hızal, “Influence of elevated temperatures on the mechanical properties and microstructure of self consolidating lightweight aggregate concrete,” *Constr. Build. Mater.*, vol. 34, pp. 575–583, Sep. 2012, doi: 10.1016/j.conbuildmat.2012.02.088.
[31] M. B. Karakoç, “Effect of cooling regimes on compressive strength of concrete with lightweight aggregate exposed to high temperature,” *Constr. Build. Mater.*, vol. 41, pp. 21–25, 2013, doi: 10.1016/j.conbuildmat.2012.11.104.
[32] R. Felicetti, P. G. Gambarova, and P. Bamonte, “Thermal and mechanical properties of light-weight concrete exposed to high temperature,” *Fire Mater.*, vol. 37, no. 3, pp. 200–216, Apr. 2013, doi: 10.1002/fam.2125.
[33] M. Yoon, G. Kim, G. C. Choe, Y. Lee, and T. Lee, “Effect of coarse aggregate type and loading level on the high temperature properties of concrete,” *Constr. Build. Mater.*, vol. 78, pp. 26–33, Mar. 2015, doi: 10.1016/j.conbuildmat.2014.12.096.
[34] L. H. Nguyen, A.-L. Beaucour, S. Ortola, and A. Noumowé, “Experimental study on the thermal properties of lightweight aggregate concretes at different moisture contents and ambient temperatures,” *Constr. Build. Mater.*, vol. 151, pp. 720–731, Oct. 2017, doi: 10.1016/j.conbuildmat.2017.06.087.
[35] Y. Ke, A. L. Beaucour, S. Ortola, H. Dumontet, and R. Cabrillac, “Influence of volume fraction and characteristics of lightweight aggregates on the mechanical properties of concrete,” *Constr. Build. Mater.*, vol. 23, no. 8, pp. 2821–2828, Aug. 2009, doi: 10.1016/j.conbuildmat.2009.02.038.
[36] “Recommendation of RILEM TC 200-HTC: mechanical concrete properties at high temperatures—modelling and applications | SpringerLink.” https://link.springer.com/article/10.1617/s11527-007-9286-1 (accessed Nov. 12, 2019).
[37] J. J. Kollek, “The determination of the permeability of concrete to oxygen by the Cembureau method—a recommendation,” *Mater. Struct.*, vol. 22, no. 3, pp. 225–230, May 1989, doi: 10.1007/BF02472192.
[38] L. J. Klinkenberg, “The Permeability Of Porous Media To Liquids And Gases,” *Drilling and Production Practice*. American Petroleum Institute, New York, New York, 1941.
[39] M. A. Carpenter, E. K. H. Salje, A. Graeme-Barber, M. T. Dove, and K. S. Knight, “Calibration of excess thermodynamic properties and elastic constant variations associated with the $\alpha \leftrightarrow \beta$ phase transition in quartz,” *Am. Mineral.*, vol. 83, no. 1, pp. 2–22, Jan. 1998, doi: 10.2138/AM-1998-0101.
[40] N. R. Rijaniaina, “Comportement des bétons à haute temperature : Influence de la nature du granulat,” Université Cergy-Pontoise, 2015.
[41] A. N. Noumowe, P. Clastres, G. Debicki, and J.-L. Costaz, “Transient heating effect on high strength concrete,” *Nucl. Eng. Des.*, vol. 166, no. 1, pp. 99–108, 1996, doi: 10.1016/0029-5493(96)01235-6.
[42] U. Schneider, U. Diederichs, and C. Ehm, “Effect of temperature on steel and concrete for PCRV’s,” *Nucl. Eng. Des.*, vol. 67, no. 2, pp. 245–258, 1982.
[43] S. Real and J. A. Bogas, “Oxygen permeability of structural lightweight aggregate concrete,” *Constr. Build. Mater.*, vol. 137, pp. 21–34, Apr. 2017, doi: 10.1016/j.conbuildmat.2017.01.075.
[44] H. Carré, C. Perlot, A. Daoud, M. J. Miah, and B. Aidi, “Durability of Ordinary Concrete after Heating at High Temperature,” *Key Eng. Mater.*, vol. 711, pp. 428–435, Sep. 2016, doi: 10.4028/www.scientific.net/KEM.711.428.
[45] E. Hwang, G. Kim, G. Choe, M. Yoon, N. Gucunski, and J. Nam, “Evaluation of concrete degradation depending on heating conditions by ultrasonic pulse velocity,” *Constr. Build. Mater.*, vol. 171, pp. 511–520, May 2018, doi: 10.1016/j.conbuildmat.2018.03.178.
[46] W. P. S. Dias, Gabriel. A. Khoury, and Patrick. J. E. Sullivan, “Shrinkage of Hardened Cement Paste at Temperatures up to 670 C (1238 F),” *ACI Mater. J.*, vol. 87, no. 87, pp. 204–209, Mar. 1990, doi: 10.14359/1981.
[47] A. N. Noumowe, “Temperature distribution and mechanical properties of high-strength silica fume concrete at temperatures up to 200 C,” *Mater. J.*, vol. 100, no. 4, pp. 326–330, 2003.
[48] Y. Ke, S. Ortola, A. L. Beaucour, and H. Dumontet, “Identification of microstructural characteristics in lightweight aggregate concretes by micromechanical modelling including the interfacial transition zone (ITZ),” *Cem. Concr. Res.*, vol. 40, no. 11, pp. 1590–1600, Nov. 2010, doi: 10.1016/j.cemconres.2010.07.001.

626 [49] N. Torić, I. Boko, S. Juradin, and G. Baloević, “Mechanical properties of lightweight concrete after fire
627 exposure,” *Struct. Concr.*, vol. 17, no. 6, pp. 1071–1081, 2016, doi: 10.1002/suco.201500145.
628